EP15B-1333

New Constraints on Grain Size of Eolian Sediments in the Stimson Sandstone, Gale Crater, Mars and Implications for Paleoclimate

Sarah Preston[1*], Kirsten Siebach[1], Mathieu Gaetan Andre Lapôtre[2]

[1]Rice University Department of Earth, Environmental and Planetary Sciences; [2]Stanford University Geological Sciences; *Corresponding author, slp7@rice.edu

Introduction

- The Stimson formation (shown in Fig. 1) is a unit of cross-bedded eolian sandstone in Gale Crater, Mars that unconformably overlies the Murray mudstone and is estimated to be 3.1-3.6 Gy (Banham et al., 2018)
- Comparing ancient and modern eolian deposits on Mars enables comparison between ancient and modern conditions (Goosmann et al., 2018)
- Grain size in the Stimson is poorly constrained, though previous work has found a coarser grain size distribution in the Stimson (Banham et al., 2018) than is found in active dunes (Ehlmann et al., 2017; Weitz et al., 2018)
- This work addresses three competing hypotheses:
  - The Stimson is coarser than active dunes due to a thicker paleoatmosphere (Banham et al., 2018)
  - The Stimson has a wider grain size distribution than active dunes due to a less dense paleoatmosphere (Goosmann et al., 2018)
  - The difference in grain size between the Stimson and active dunes is controlled by sand supply, not atmospheric conditions
- Most methods used to measure grain size on Earth are not feasible on Mars, making it difficult to constrain grain size
- Weitz et al. (2018) analyzed 17 targets imaged by Curiosity's Mars Hand Lens Imager (MAHLI) to constrain the grain size distribution of eolian bedforms in the active Bagnold Dunes and found primarily well-sorted, fine size distributions

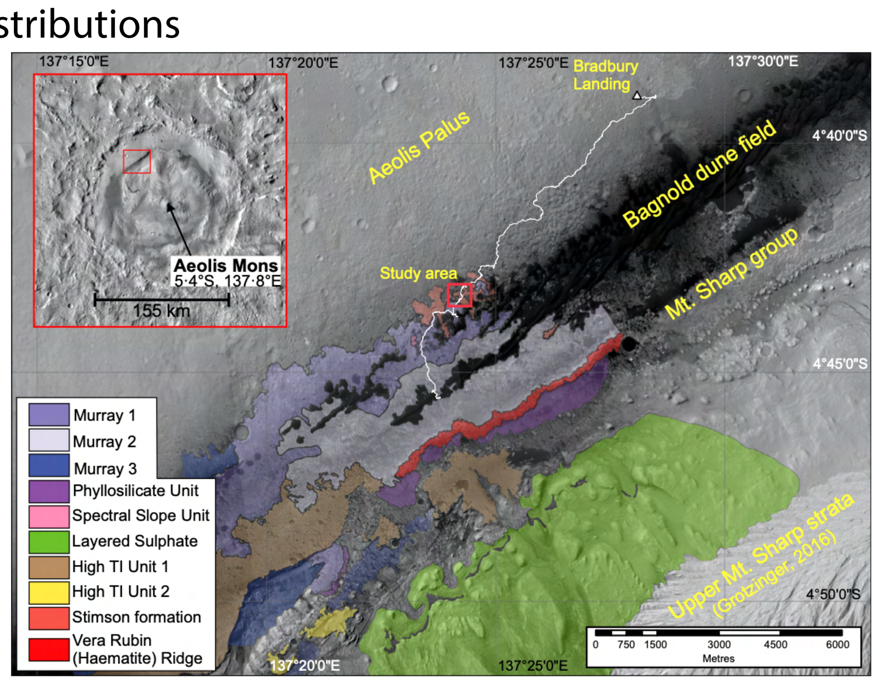

Figure 1. High Resolution Imaging Science Experiment (HiRISE) mosaic showing Curiosity's traverse to Sol 1200 with the units mapped by Fraeman et al. (2016). The red box shows the study area from Banham et al. (2018); this work covers a broader area. Figure from Banham et al. (2018).

Grain Size Measurement

- Created and used grain size card to provisionally assess and sort images (Fig. 2)
- Trained on existing data sets of cemented sandstone and loose sands from Banham et al., 2018; Ehlmann et al., 2017; Siebach et al., 2017
- Initial data set of 46 MAHLI images of 34 APXS targets in the Stimson, all with approximately 5 cm standoff (Edgett et al., 2015)
- Used ImageJ to measure largest 10 grains in each image (Schneider et al., 2012)
- Sorted targets into 9 groups based on prevalence of coarse grains (Table 1, Fig. 6)
- Selected two targets per included group (C, D, E, F, G, H) and one from group B to analyze more completely by measuring ~300 grains with the grid by number method (Banham et al., 2018; Jerolmack et al., 2006; and Kellerhals & Bray, 1971) using ImageJ (Jerolmack et al., 2006 and Weitz et al., 2018) (Fig. 7)
- Applied texture groupings to ChemCam RMIs in order to increase sample size; weighted texture groups by frequency to estimate grain size for the formation
- Grouped measurements into quarter-Φ bins, then used GRADISTAT to estimate d_{10}, d_{90}, d_{50}, and mean for each texture group and for the Stimson as a whole (Blott & Pye, 2001)

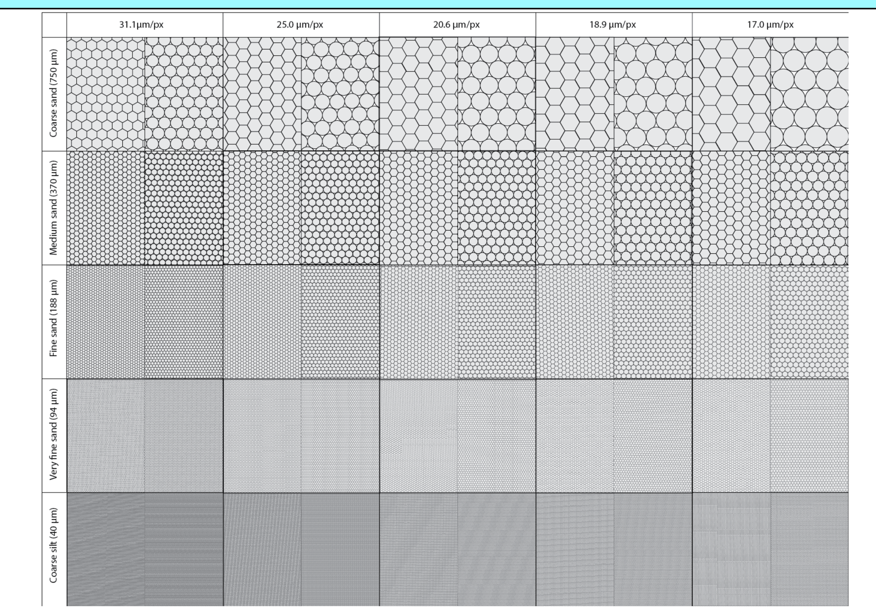

Figure 2. Grain size card for quick visual estimation of grain size distribution in MAHLI images for 5 common image scales, following the grain size classification scheme of Wentworth (1922). Circles and hexagons for each grain size and image scale enable classification of cemented and uncemented sediments. The grain size card is the same size as standard MAHLI images and must be opened at the same scale.

Figure 3. Sample images from each group described in Table 1; all images taken at ~5cm standoff.

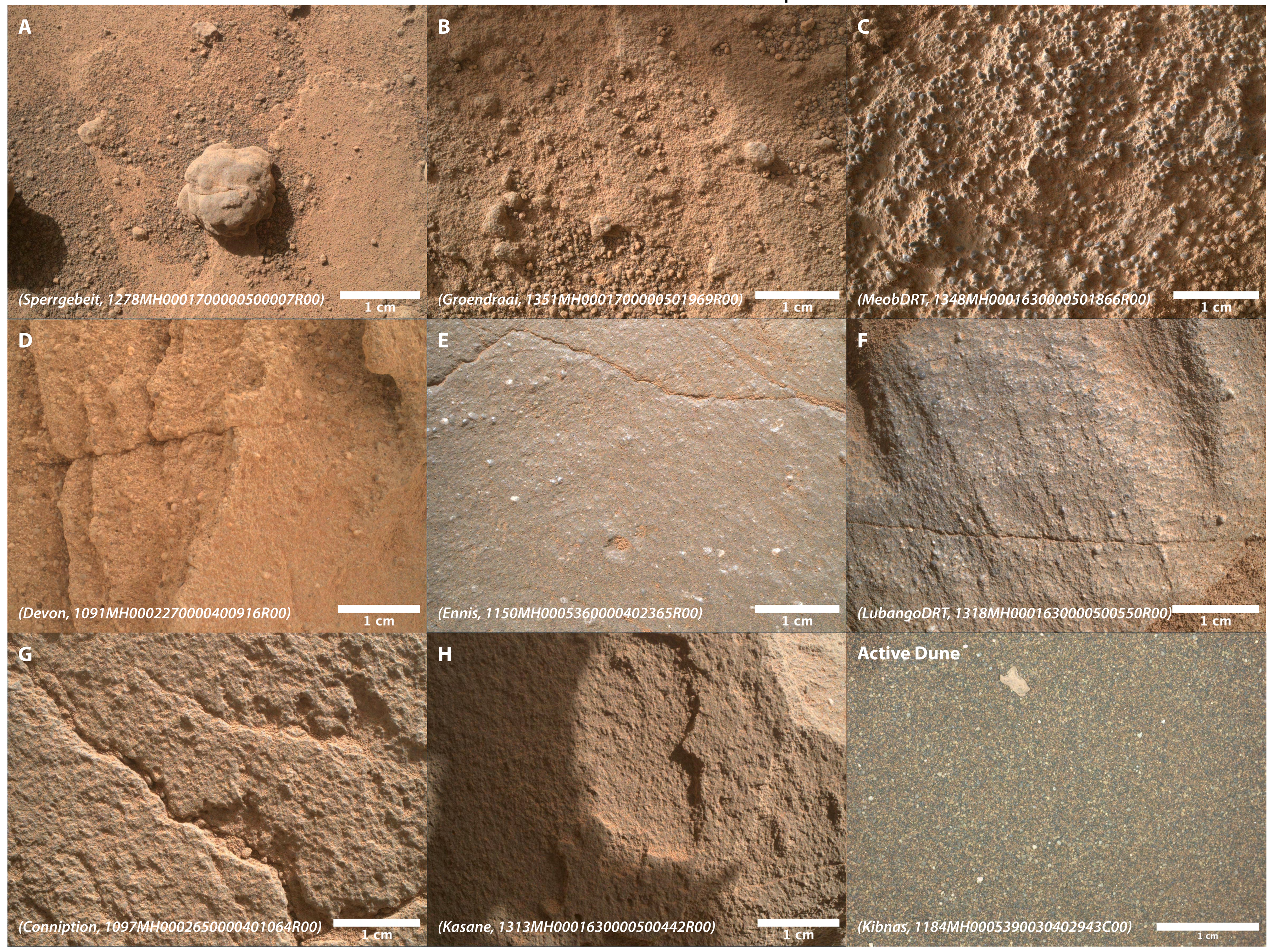

Texture Group	Description	Included	Number of Targets	Measured Targets
A	diagenetic	no	9	none
B	soils	no	2	Groendraai (1351)
C	>75% of visible grains are coarse	yes	4	MeobDRT (1348) OkorusoDRT_offset (1330)
D	25%-75% of visible grains are coarse; remainder are medium, fine, or very fine	yes	3	Ivanhoe (1092) Devon (1091)
E	between 10 grains and 25% of visible grains are coarse; remainder are medium, fine, or very fine	yes	12	BeroDRT (1300) Ennis (1150)
F	less than 10 visible grains are coarse; remainder are medium, fine, or very fine	yes	7	BrukkarosDRT (1293) LubangoDRT (1318)
G	predominantly coarse or medium that are very well cemented; few or no easily distinguishable grains	yes	4	Conniption (1097) Rossing (1288)
H	predominantly fine or very fine grains that are very well cemented; few or no easily distinguishable grains	yes	4	Kasane (1300) Vandalia (1143)
X	indeterminable texture	no	1	none

Table 1. Description of the texture classifications used in this work to sort MAHLI images for more detailed grain size measurements and to extrapolate the frequency of various textures throughout the Stimson formation.

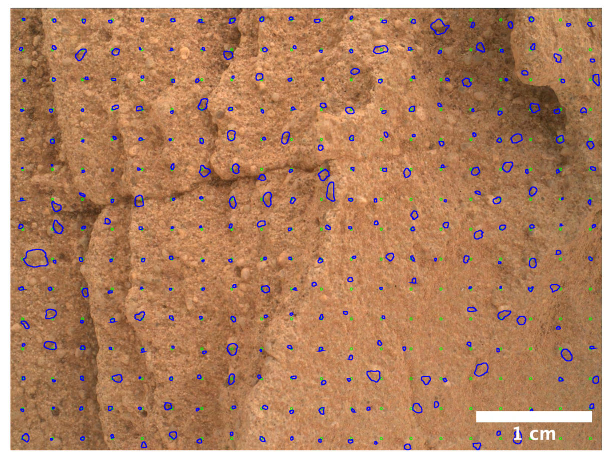

Figure 4. MAHLI image with 80px grid (green) and grain outlines (blue). The closest grain to each grid point is outlined; if there are no distinct grains, a grain at the smallest resolvable size is recorded.

Results and Conclusions

- The grain size card measurements, measurements from past work, and ImageJ measurements from this work agree well (Banham et al., 2018; Ehlmann et al., 2018; Siebach et al., 2017)
- While the finer fraction is difficult to resolve in cemented targets, the Stimson's coarsest grains are coarser than those in Bagnold Dune sand (Fig. 8) (Ehlmann et al., 2017; Weitz et al., 2018)
- Although denser atmospheres facilitate the initiation of saltation via wind drag, less dense atmospheres enhance transport hysteresis such that transport may be sustianed under low wind speeds once it is initiated. Modern winds are not predicted to initiate saltation through fluid drag; however, grains are transported in the modern atmosphere, suggesting that transport initiation likely occurs at wind speeds below the fluid threshold (Sullivan and Kok, 2017)
- As a result, observations of the Stimson do not require a denser paleoatmosphere

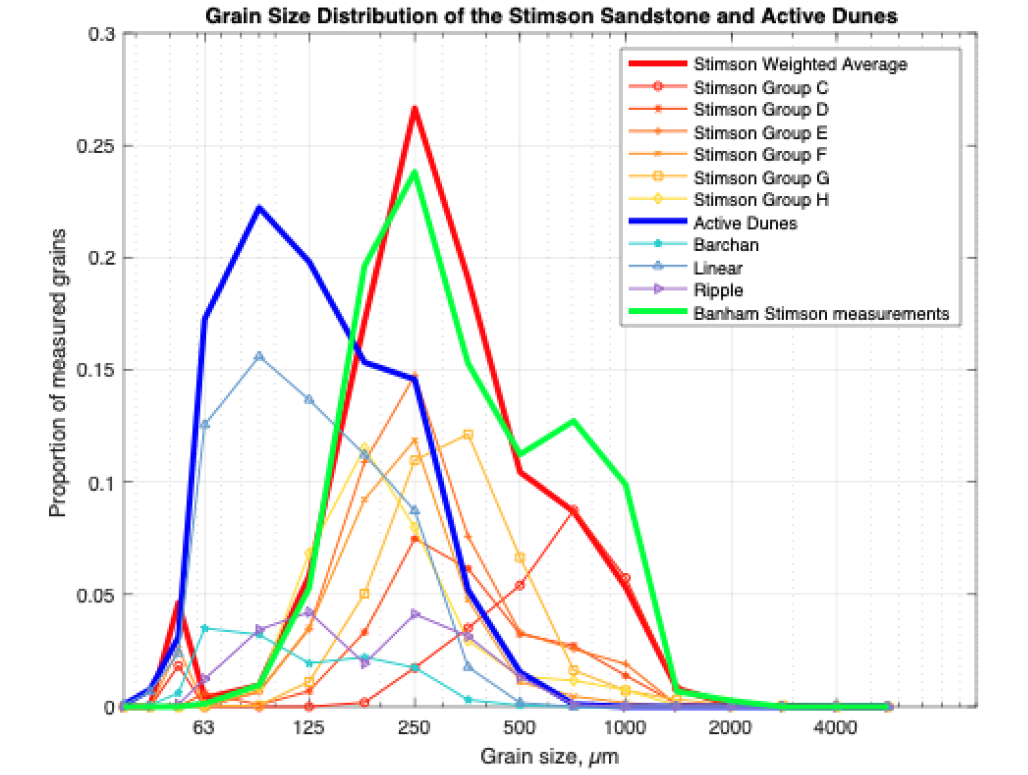

Figure 8. Grain size distribution of the Stimson sandstone from this work (red) and Banham et al. (2018) (green), as well as the grain size distribution of active dunes from Ehlmann et al. (2017) and Weitz et al. (2018) (blue).

Future Work

- Though further work is needed, observations do not appear to require a denser atmosphere; a different sand source may explain the comparatively coarse grain size distribution of the Stimson
- Mastcam imagery will allow us to to analyze geomorphological features indicative of wind speed and to refine MAHLI data set to study other transport populations
- Comparing grain composition, mineralogy, sorting, and shape between active dunes and the Stimson will provide insight on the provenance and transport of the Stimson formation

Grain Size and Eolian Transport

- Grain transport is described by a set of experimentally determined equations, graphed in Fig. 5, Fig. 6:
  - Equation 1 gives the threshold friction velocity u^*_t, the shear velocity at which grains begin to move (Shao & Lu, 2000, following Iversen & White, 1982)
  - Equation 2 gives the impact threshold velocity u^*_i, the shear velocity at which grains continue to move once motion has initiated (Kok, 2010)
  - Equation 3 gives the fluid density as a function of atmospheric pressure and temperature

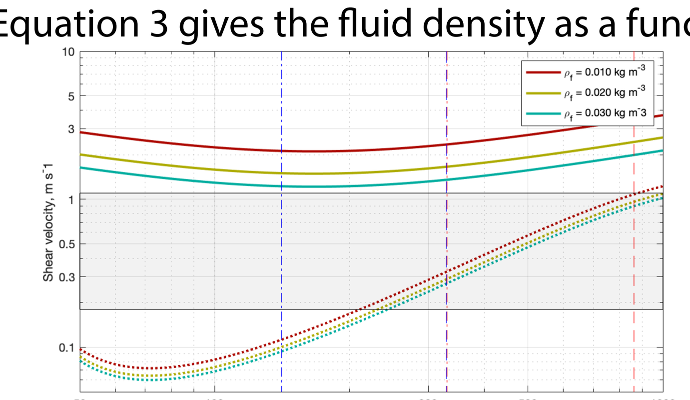

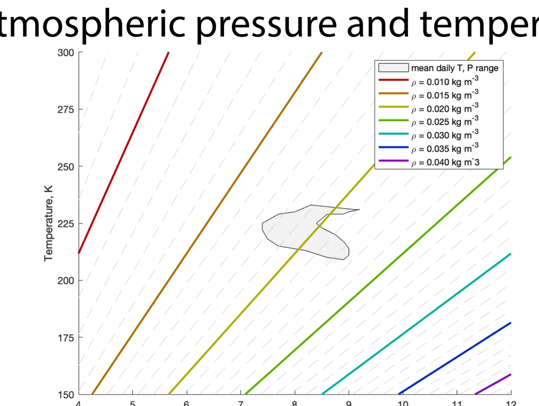

Figure 5 (left). Graph of threshold friction velocity u^*_t (solid lines) and u^*_i (dotted lines, setting T = 225 K) as a function of grain diameter for some of the fluid densities shown in Figure 6. The shaded area shows u^*_{modal} - u^*_{max} (Viúdez-Moreiras et al., 2019); the dotted and dashed vertical lines show the d_{50} and d_{90}, respectively, of the Bagnold Dunes (blue, Ehlmann et al., 2017, and Weitz et al., 2018) and the Stimson (red).

Figure 6 (right). Contours of constant ρ_f as a function of pressure and temperature. The gray polygon represents the mean daily pressure and temperature in Gale Crater over a period of 3 Martian years (Martínez et al., 2017).

Figure 7 (bottom right). The three dominant modes of grain transport. Modified from Jerolmack et al. (2006).

$$(1)\qquad u^*_t = \sqrt{0.0123\left(\frac{\rho_s g d}{\rho_f} + \frac{\gamma \,\mathrm{kg\,s^{-2}}}{\rho_f d}\right)}$$

$$(2)\qquad u^*_i = c_1\left(\frac{700 M_{CO_2}}{\rho R T}\right)^{\frac{1}{6}}\left(\frac{220}{T}\right)^{\frac{2}{5}}\exp\left[\left(\frac{c_2}{d}\right)^3 + c_3\sqrt{d} - c_4 d\right]$$

$$(3)\qquad \rho_f = \frac{P M_{CO_2}}{RT}$$

g = gravity = $3.72\ \mathrm{m\,s^{-2}}$
ρ_s = solid density = $2900\ \mathrm{kg\,m^{-3}}$
$c_1 = 5.5 \times 10^{-3}\ \mathrm{m\,s^{-1}}$
$c_2 = 49\ \mu\mathrm{m}$
$c_3 = 0.29\ \mu\mathrm{m}^{-0.5}$
$c_4 = 3.84 \times 10^{-3}\ \mu\mathrm{m}^{-1}$
γ = an experimentally derived constant = $3.0 \times 10^{-4}\ \mathrm{kg\,s^{-2}}$ (following Jerolmack et al., 2006)
R = the gas constant = $8.3145\ \mathrm{J\,mol^{-1}\,K^{-1}}$
M_{CO_2} = the molar mass of carbon dioxide = $0.044009\ \mathrm{kg\,mol^{-1}}$

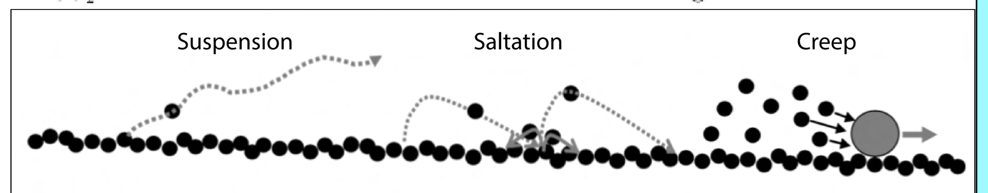

- There are three dominant modes of of grain transport, (Fig. 8, Eastwood et al., 2012; Jerolmack et al., 2006):
  - Suspension, in which grains become entrained in the fluid flow and travel distances of many grain diameters; wind speed **$u^* > $ settling velocity w_s**
  - Saltation, in which grains move ballistic trajectories and dislodge other particles in the bed; **$u^* > u^*_t$** to initiate transport, **$u^* > u^*_i$** to continue
  - Creep, in which grains that are too large to move in saltation slide or roll, driven by saltating grains; on Earth, **$0.7u^*_t \leq u^* < u^*_t$**
- This work focuses on saltation

Acknowledgements

The Gerald R. Soffen Memorial Fund Travel Grant

References

Banham, S. G. et al. (2018) Sedimentology, 65(4), 993-1042; Blott, S. J. & Pye, K. (2001) ESPL, 26(11), 1237-1248; Eastwood, E. N, et al. (2012) JGR, 17(F3); Edgett, K. et al. (2015) MSL MAHLI Technical Report 0001; Ehlmann, B. L. et al. (2017) JGR, 122(12), 2510-2543; Fraeman, A. A. et al. (2016) JGR, 121(9), 1713-1736; Goosmann, E. A. et al. (2018) JGR, 123(10), 2506-2526; Iversen, J. D. & White, B. R. (1982) Sedimentology, 29(1), 111-119; Jerolmack, D. J. et al. (2006) JGR, 111 (E12). Kellerhals, R. & Bray, D. I. (1971) Journal of the Hydraulics Division, 97(8), 1165-1180; Kok, J. F. (2010) GRL, 37(12); Martínez, G. M. et al. (2017) SSR, 212(1), 295-338; Schneider, C. A. et al. (2012) Nature Methods, 9(7), 671-675; Shao, Y. & Lu, H. (2000). JGR, 105(D17), 22437-22443; Siebach, K. L. et al. (2017) JGR, 122(2), 295-328; Sullivan, R. and Kok, J. F. (2017) JGR, 122(10), 2111-2143; Viúdez-Moreiras, D. et al. (2019) Icarus, 399, 645-656; Weitz, C. M. et al. (2018) GRL, 45(18), 9471-9479; Wentworth, C. K. (1922) The Journal of Geology, 30(5), 377-392.